JOURNAL OF MATERIALS SCIENCE 28 (1993) 1074–1080

The role of elastic property mismatch in the failure of ceramic composites

JOW-LAY HUANG, CHING-JANG LIN
Department of Materials Engineering, National Cheng-Kung University, Tainan, Taiwan

Numerical analysis was undertaken to simulate a modification of the normalized stress-intensity factor applicable when the crack tip is in the vicinity of an interface separating materials of differing elastic properties. It is predicted that when the initial crack is subcritically extended to the interface, the strength of the sample is greater than if the failure occurred from the initial crack, without arrest at the interface. The fracture behaviour of microcracking on a polished WC/Si_3N_4 sample was examined. Crack branching, deviation and arrest were observed to depend on the instantly released energy.

1. Introduction

In most ceramics of practical interest, the size of microcracking leading to ultimate failure is comparable with that of microstructural inhomogeneities. The latter, which could alter the behaviour of a microcrack, consist of (1) internal stress arising from anisotropy in thermal expansion along different crystallographic directions, (2) second-phase inclusion having different elastic and thermal expansion characteristics by comparison with the matrix, and (3) duplex microstructure consisting of a few large grains in a matrix of otherwise fine grains. Our work is focused on the influence of a second phase on the fracture behaviour of microcracking which is of particular significance in relation to delayed failure in a ceramic composites.

The influence of second-phase particles on fracture has been previously examined [1–3]. Interaction of a crack front with second-phase particles has also been examined with regard to the mismatch of elastic properties [4, 5]. In some investigations, the influence of elastic property mismatch was incorporated by means of the principle of superposition [4–6]. Some researchers also proposed that the stress intensity factor exhibits a singularity when the tip is at the interface; specifically when a crack tip contained in a material of smaller modulus approaches an interface separating a body of larger modulus, the normalized stress-intensity factor decreases to zero [7–9].

Numerical calculations have been performed which take into account the modification of normalized stress-intensity factor near the interfaces. Microcracking was introduced by a Vickers diamond-tip indentor on a polished surface of silicon nitride-containing tungsten carbide which has an extremely high elastic modulus and toughness among ceramics. SEM was used to examine crack behaviour, and observations were compared with the results of numerical analysis.

2. Numerical analysis

2.1. Model

The numerical model is based on a specimen as shown in Fig. 1. The initial crack was assumed to have the shape of a half-penny of radius c_0 contained in Material 1, which has the physical properties of borosilicate glass (Corning 7570 glass: 75% PbO, 11% Al_2O_3, 11% B_2O_3, 3% SiO_2). The radius of Material 1 was $r = 350$ μm. The physical properties of Material 2 in this model were based on a Corning glass ceramic (Macor). K_{Ic} of materials 1 and 2 were experimentally determined by the double cantilever beam technique. Crack growth parameters were determined by dynamic fatigue tests for both materials. The properties of concern for numerical analysis are listed in Table I. Materials were chosen to give substantial variation in elastic modulus and toughness but with similar thermal expansion coefficients. Stress rates were calculated for a four-point bend specimen with square cross-section dimensions of 5 mm in a Universal testing machine under fixed loading rates.

2.2. Energy balance analysis

In specimens in which the initial crack becomes critical ($K_I \geqslant K_{IC}$) before the crack reaches the interface, the crack begins to propagate rapidly. A true dynamic analysis of such a problem is currently unavailable because the stress-intensity factor near the interface under dynamic conditions is unknown. We therefore used the quasistatic analysis proposed by Mott [10] and used by Berry [11] and Singh [12]. In the use of quasistatic analysis, we assume that the velocity reached by a crack is less than 10% of the Rayleigh wave speed.

Energy balance analysis, in which the strain energy, the surface energy and the kinetic energy are assumed

0022–2461 © *1993 Chapman & Hall*

to be the only forms of energy, was used to estimate the arrest crack length, C_a.

As K_I reaches K_{IC}, the initial crack begins to propagate rapidly. After the crack crosses the interface, it enters a region of increased resistance. The energy balance was carried out for fixed grips condition. The only forms of energy assumed were strain, surface and kinetic energy. As no energy was assumed to be lost to the surroundings, the initial energy (when the crack just began to propagate rapidly) which consists of strain and surface energies is equal to the final energy (when the rapidly propagating crack is arrested), which also consists of strain and surface energies; that is

$$U_1(C_1) + S_1(C_1) = U_a(C_a) + S_a(C_a) \quad (1)$$

in which C_1 is the crack length at which K_I reached $K_{Ic(1)}$, C_a is the arrest crack length, $U_{1,a}$ the corresponding strain energies, and $S_{1,a}$ the corresponding surface energies. The strain energies consist of two terms: one is independent of crack length, which was determined using the beam theory. The other term depends on the crack length, which was obtained from three-dimensional crack theory. Equation 1 was solved numerically according to Singh [12]. A real positive root for C_a indicates crack arrest. If no real positive root exists for C_a, according to the quasistatic analysis, the crack completely propagates through the body.

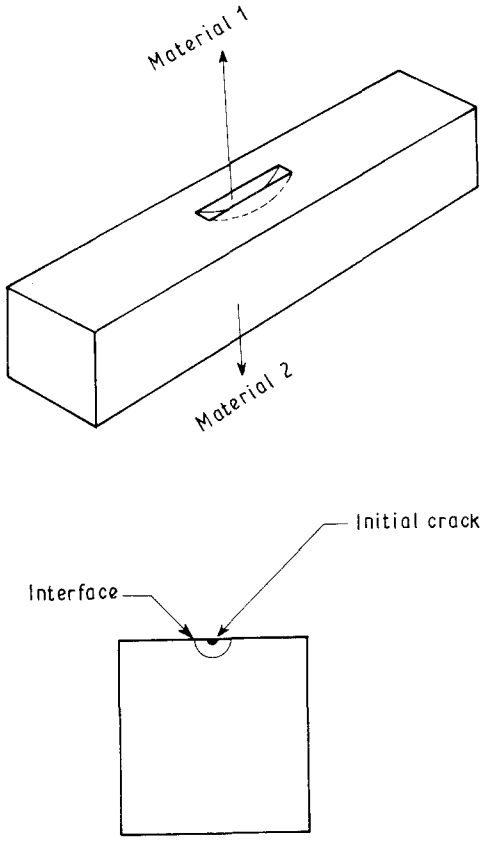

Figure 1 Schematic drawing of the composite model.

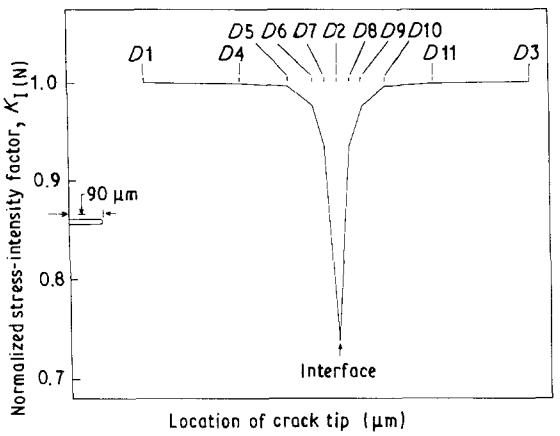

Figure 2 $K_{I(N)}$ versus crack length used in the calculation of static and dynamic fatigue curves.

In Table II, the initial (at which $K_I = K_{Ic(1)}$) and the arrest crack lengths are given for various initial crack lengths for a fixed fillet size ($r = 350$ μm). The overshoot length is generally small. With progressively smaller initial crack lengths, the overshoot becomes progressively larger. When the initial (at which $K_{Ic} = K_{Ic(1)}$) crack length is small enough, failure occurs from the initial crack and the effect of the interface is not seen by the crack. This phenomenon is essential for the toughness of composites.

The behaviour of a crack near an interface can be analysed only if the variation of $K_{I(N)}$ with crack length is known. Our objective is to evaluate qualitatively the behaviour of a crack near the interface; therefore, we assume the relationship for $K_{I(N)}$ with respect to C (crack length) based on Erdogan's work [13, 14]. This variation of $K_{I(N)}$ versus C is shown in Fig. 2. $K_{I(N)}$ is defined as

$$K_{I(N)} = \frac{K_I}{\left(\frac{2}{\pi^{1/2}}\sigma c^{1/2}\right)} \quad (2)$$

such that for a crack in the shape of a half-penny, $K_{I(N)} = 1$ when the crack tip is far from the interface. The variation of $K_{I(N)}$ with crack length has been approximated by straight segments to simplify the numerical procedure. The relationships for crack velocity versus stress intensity factor for both Materials 1 and 2 are given by

$$V = A_1 K_I^{N_1} \quad (3)$$

TABLE I Physical properties of Material 1 and 2 used for numerical analysis

	Young's modulus, E (MN M^{-2})	Critical stress intensity factor, K_{Ic} (MN m$^{-3/2}$)	Thermal expansion coefficient, α (10^{-6} °C^{-1})
Material 1	5.5×10^4	0.64	9
Material 2	6.5×10^4	1.40	9

TABLE II The initial (at which $K_I = K_{Ic(1)}$) and the arrest crack length for various initial crack lengths for a fixed fillest size

initial crack radius, C_o (μm)	Arrest crack radius, C_a (μm)
326	350.3
308	351
293	352
282	353
273	354
266	355
259	356
253	357
248	358
243	359
238	360
237	361
≲225	No positive root. Failure occurred from the initial crack

and

$$V = A_2 K_I^{N_2} \tag{4}$$

The stress in Material 1 is given by

$$\sigma_1 = \left(\frac{E_1}{E_2}\right)\sigma \tag{5}$$

in which σ is the stress in Material 2, and E_1 and E_2 are Young's moduli of elasticity for Materials 1 and 2, respectively. N_1 and N_2 are the respective parameters for slow crack growth. For the variation of $K_{I(N)}$ shown in Fig. 2, K_I for a given stress, σ, is expressed

$$K_I = \frac{E_1}{E_2}\frac{2}{\pi^{1/2}}\sigma C^{1/2} K_{I(N)} \quad \text{for } C \leqslant D_2 \tag{6}$$

$$K_I = \frac{2}{\pi^{1/2}}\sigma C^{1/2} K_{I(N)} \quad \text{for } C \geqslant D_2 \tag{7}$$

By definition we have defined K as

$$K_I = \left(\frac{E_1}{E_2}\right)\frac{2}{\pi^{1/2}}\sigma C^{1/2} K_{I(N)} \tag{8a}$$

when the crack tip is contained in Material 1, whereas

$$K_I = \frac{2}{\pi^{1/2}}\sigma C^{1/2} K_{I(N)} \tag{8b}$$

when the tip is in Material 2.

Numerical calculations were conducted to generate a curve for dynamic fatigue with $K_{I(N)}$ versus C shown in Fig. 2.

Numerical calculations were performed with C_o (initiation crack) = 90 μm. The instantaneous applied stress is $\sigma = \dot{\sigma} \times t$ in which $\dot{\sigma}$ is the stressing rate and t is the cumulative time. The magnitudes of D_1 and the slopes of the straight segments in the $K_{I(N)}$ plot are shown in Fig. 2.

For a given initial crack size, C_o, and a given stress rate, $\dot{\sigma}$, σ and K_I were determined using the $K_{I(N)}$ plot shown in Fig. 2. Subsequently, the crack velocity and the period required for the crack to grow a small increment, 0.1 μm, were also determined (Δt). At the end of this step, K_I was calculated for the new crack length, $C_o + \Delta C$, and once again the period required for an additional increment ΔC was determined. This procedure was continued until either the $K_{Ic(1)}$ was reached or the crack reached the interface.

If $K_{Ic(1)}$ was reached prior to the crack arriving at the interface, the energy-balance analysis given by Singh *et al.* [12] was conducted. For this analysis, the new crack length at which K_I reached $K_{Ic(1)}$ is the initial crack length C_1. Using the energy balance analysis, we determined the arrested crack length, C_a, in Material 2.

If no positive root greater than D_2 was found, the crack did not arrest and failure occurred. Then the cumulative period of crack growth from C_o to C_1 is the total failure period; if a real positive root greater than D_2 is found, this root gives C_a which is the new initial crack length C_1. Again the period Δt required for an increment $\Delta C = 0.1$ μm was determined using the v–k characteristics of Material 2. The calculations were continued until K_I reached $K_{Ic(2)}$ at which instant failure occurred. Fig. 3 is a flow chart of the computer program.

In Fig. 4, the crack velocity is shown as a function of the location of the crack tip for two values of the stress rate. For these two values, K_I never reached $K_{Ic(1)}$ and thus the crack grew slowly to the interface.

Numerical calculations were further carried out to determine K_I as a function of the location of the crack tip (Fig. 5). Behaviour of three types was again observed. With the initial crack size, $C_o = 90$ μm, for a high loading rate, failure occurred from Material 1 without crack arrest. For smaller values of the stress rate ($\dot{\sigma} \approx 0.8$ and 2.0 MPa s^{-1}) although K_I reached $K_{Ic(1)}$ in Material 1, the crack arrested just across the interface after rapid crack propagation. Subsequently, subcritical crack growth occurred in Material 2. For an even smaller loading rate ($\dot{\sigma} \approx 0.02$ MPa s^{-1}), K_I never reached $K_{Ic(1)}$; the crack approached the interface subcritically crossed it and, after subcritical crack growth in Material 2, failure occurred. In this case also, the crack tip passed a substantial period at the interface. However, as the stress continually increases, K_I for an arrested crack increases even though the crack length remains essentially unchanged. This effect leads to a discontinuity in the plot of K_I versus the location of the crack tip shown in Fig. 5.

A numerically generated rate curve for strength versus stress rate appears in Fig. 6. Region I indicates that failure occurred from Material 1, and Region III indicates that the crack grew slowly to the interface. The strength increases with increasing loading rate in both regions. Note that the strength is greater at smaller loading rates (Region III), this is opposite to what is known in a monolithic material.

In Region II, in which the initial crack propagated rapidly and arrested in Material 2, the strength actually decreases with increasing stressing rate over a range of loading rates.

3. Experimental procedure

In the previous quasistatic analysis, we have shown pronounced effects of mismatch of elastic properties across an interface on a relatively slowly propagating

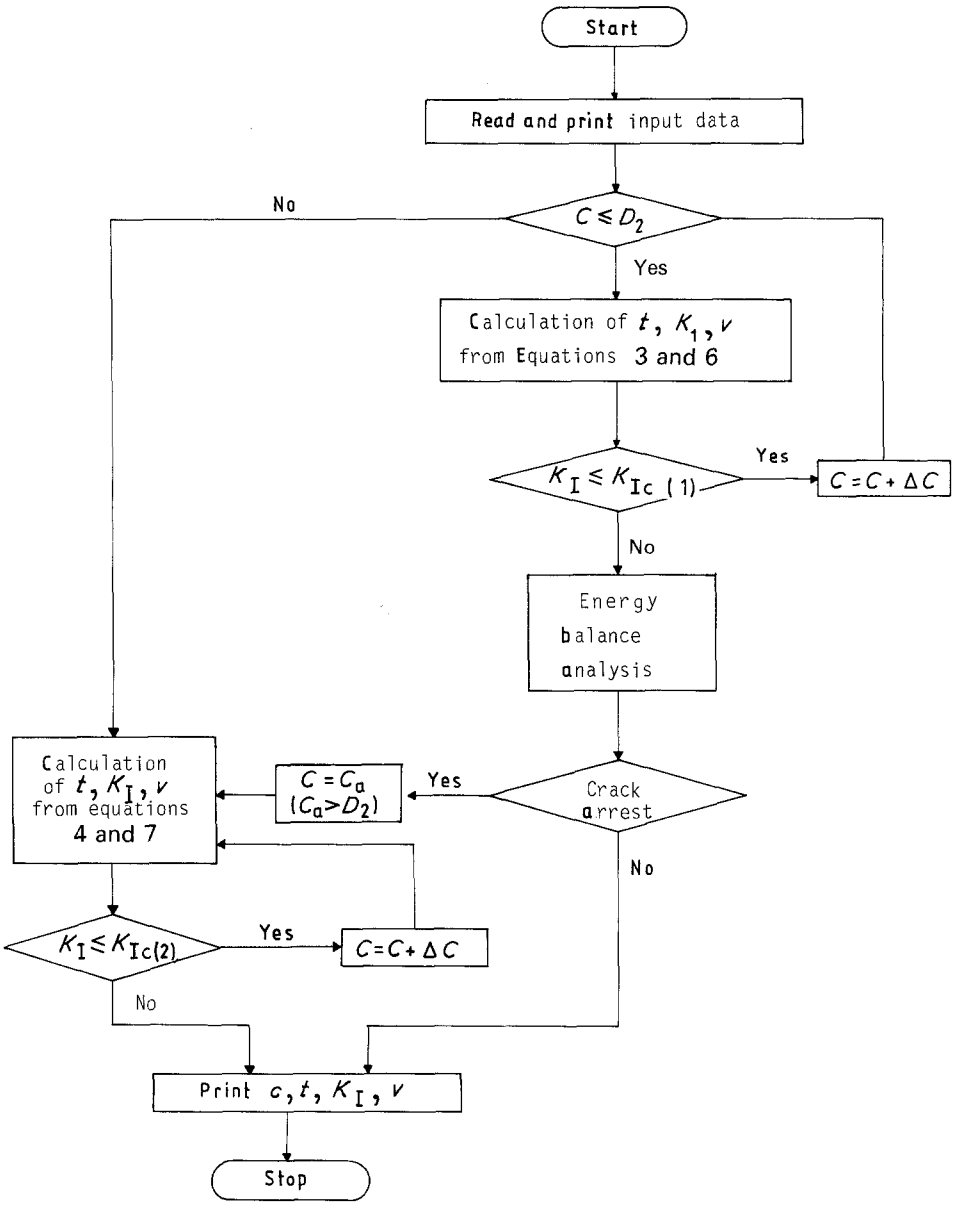

Figure 3 Flow chart of the computer program used in numerical analysis.

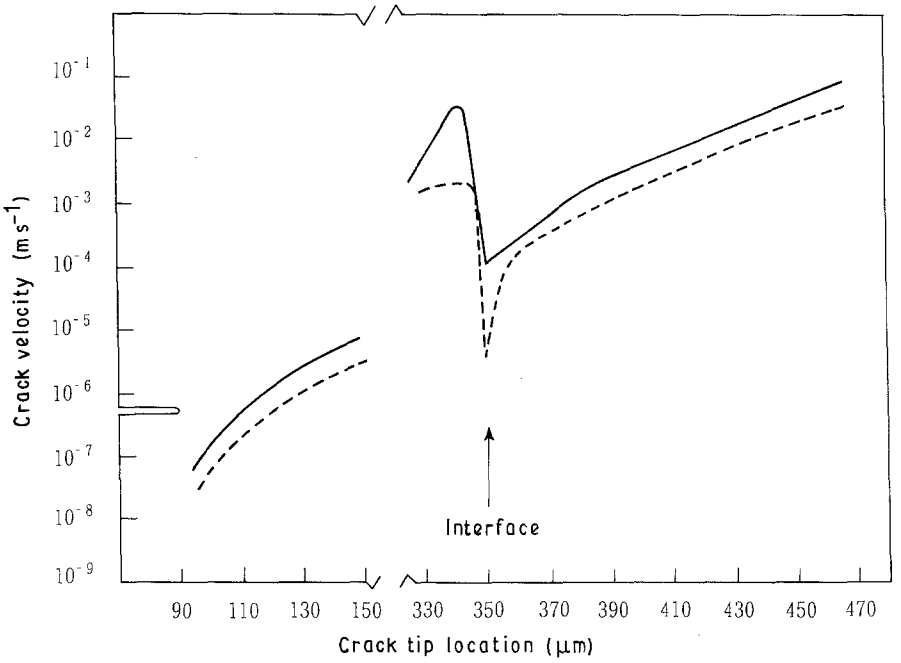

Figure 4 Calculated crack velocity versus crack length for (——) $\dot{\sigma} = 2 \times 10^4$ Pa s^{-1} and (– – –) $\dot{\sigma} = 8 \times 10^3$ Pa s^{-1}.

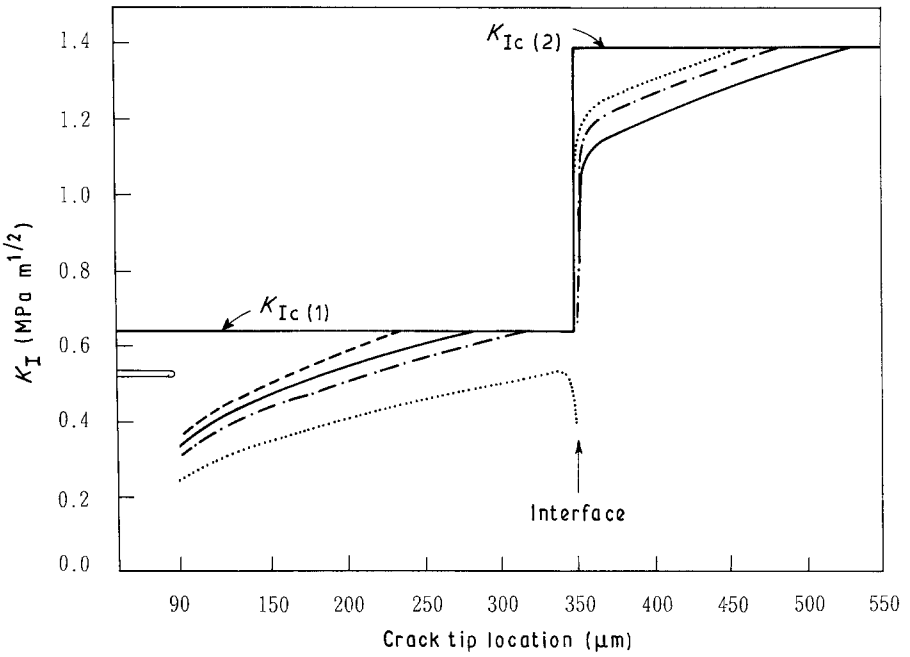

Figure 5 Calculated K_I versus crack length for various stressing rates. $\dot{\sigma}$; (– – –) 10 MPa s^{-1}, (——) 2 MP s^{-1}, (– · –) 0.8 MPa s^{1}, (· · ·) 0.02 MPa s^{-1}.

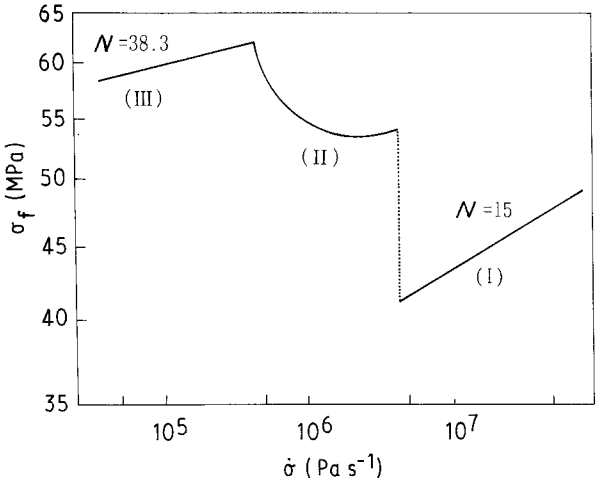

Figure 6 Calculated dynamic fatigue curves.

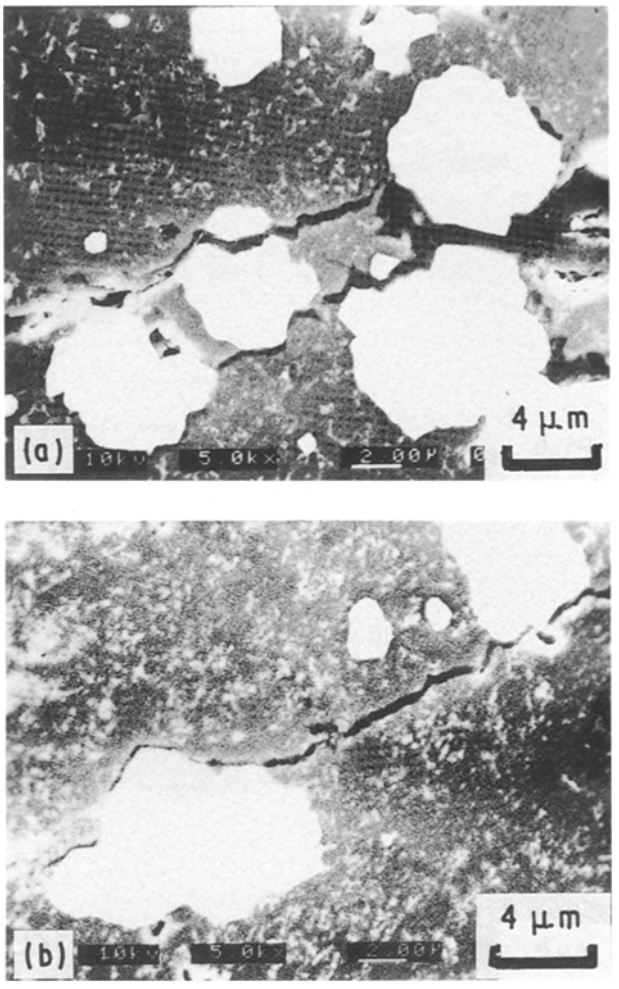

Figure 7 (a) Crack branching and (b) deflection in a WC/Si_3N_4 sample.

microcrack. In the analysis we assumed the length of the interface that separates two materials with different elastic moduli was infinite in order to simplify calculations. However, in a real ceramic matrix composite, the toughening material with large elastic modulus might be dispersed particles with limited interfacial area. Other than elastic modulus, thermal stress, geometrical shapes and boundary phases might also be involved and make an exact numerical simulation difficult.

A simple, quick experiment was then conducted in order to examine directly the behaviour of a microcrack as it approaches an interface from a ceramic matrix having relatively small modulus to a particle with a large modulus. Tungsten carbide, which has one of the largest elastic moduli (620 GPa) and toughness (10.8 MPa m$^{1/2}$) among ceramics, was chosen for the dispersed phase (Material 1) and silicon nitride (E = 410 GPa) for the matrix (Material 2).

3.1. Procedures

Silicon nitride (Si_3N_4, HCST LC-12-N) yttria (Y_2O_3, Molycorp 5603) (6 mass %) and alumina (2 mass %

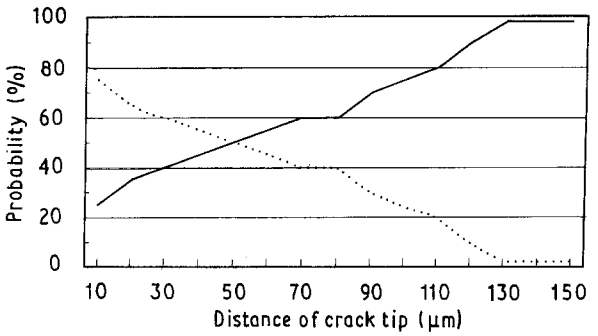

Figure 8 Probability of (···) crack branching and (——) deflection as a function of distance from the crack tip.

Al_2O_3, Alcoa 16SG) powders were milled in anhydrous ethanol with alumina grinding media (ratio of ball to charge is 7:1) for 22 h. Various compositions of tungsten carbide (WC, Elecmat WC-2, WC-9) (sizes 2 and 9 μm) were then added to the mill jar and milling continued for a further 2 h. The slurry was dried on a large, preheated plate almost instantly to avoid the rapid sedimentation of WC particles. Agglomerates were screened through a 200 mesh screen, cold isostatic pressed to 15×10^3 p.s.i. (10^3 p.s.i. $\equiv$ 6.89 N mm^{-2}), pressed into bars, buried in covering powders and sintered at 1850 °C for 2 h in a nitrogen atmosphere. Theoretical densities of 92%–99% were obtained. There was no evidence of chemical reaction between WC and Si_3N_4 under our experimental conditions.

Sample surfaces were finely polished to 1 μm before a microcrack was introduced by a Vickers diamond-tip indentor with a load of 50 kgf. An optical microscope and SEM were used to examine the whole crack propagating path, especially the interfaces between WC and Si_3N_4.

3.2. Observations and discussion

Both crack branching and crack deviation were observed along the crack propagation path (Fig. 7). The frequency of branching and deviation were counted and plotted against distance from the indentation tip based on observations from eight microcracks (Fig. 8). While the microcrack began to propagate branching appeared to be the major mechanism of failure. However, as the crack propagated further from the diamond indent, crack deflection became the dominant mechanism. Finally, crack tips were either arrested by a TiB_2 particle or a long β-silicon nitride grain.

The previous numerical analysis has shown that when a microcrack grew from a material with small modulus material to a material with large modulus, a crack could cause instant failure if k_I reached $K_{Ic(1)}$; it could also be arrested at the interface if the crack was subcritically extended to the interface before it reached $K_{Ic(1)}$. In other words the crack could either cut through Material 2 or be arrested by the interface, depending on the instantly released strain energy.

Similarly, when an indentation crack was introduced on sample surfaces experimentally, the crack could run through secondary phases of greater modulus (branching) if the instantly released strain energy was greater than the energy consumption from newly created surfaces. As the crack propagated away from the indent, progressively more kinetic energy was consumed (the total elastic energy was assumed to be constant); cracks were then either deflected (because Material 2 is a spherical particle as opposed to an infinite inferface in our numerical model) or be arrested by the secondary phases.

The previous discussion also indicates that in cases in which differences in Young's moduli between two phases is not large, effects of a material of large modulus might not be substantial for rapid fracture. The toughening effects are essential in a fracture having slow crack growth such as time-dependent static fatigue or dynamic fatigue with a slow rate of stress.

4. Conclusion

Our numerical analysis was based on the assumption that when a crack contained in a body of smaller Young's modulus approaches an interface separating a body of larger modulus, the normalized stress-intensity factor decreases. The results indicate that the crack could either fail from the material of small modulus or be arrested by the material of large modulus, depending on the instantly released strain energy at failure. The strength of a composite specimen was increased when the initial crack was subcritically extended to arrest at the interface.

Microcracking was introduced on a polished WC/Si_3N_4 specimen and fracture behaviour was examined along the crack propagation path by means of SEM and optical microscopy. Crack branching, crack deviation and arrest were observed depending on the location of the crack path. Observations were compared with the results of the numerical analysis.

Acknowledgements

We thank Professor Anil V. Virkar, University of Utah, without whose ideas and helpful discussion this report would not have been completed. We also thank the National Science Council, Taiwan, for grant NSC-79-0405-E-006-27.

References

1. SERGEJ T. BUJAN and G. J. BALDONI, *Ceram. Bull.* **66** (1987) 347.
2. K. R. KARASAK, M. R. MARTIN, G. C. YEN and J. L. SCHIENLE, *J. Amer. Ceram. Soc.* **72** (1989) 628.
3. RAMAKRISHNAN T. BHATT, *Ceram. Engng Sci. Proc.* **11** (1990) 974.
4. J. TIROSH and A. S. TETELMAN, *Int. J. Fract.* **12** (1976) 187.
5. D. J. GREEN and P. S. NICHOLSON, in "Fracture Mechanics of Ceramics", edited by R. C. Bradt, D. P. H. Hasselman and F. F. Lange (Plenum Press, New York, 1978) pp. 945–60.
6. R. W. DAVIDGE and T. J. GREEN, *J. Mater. Sci.* **3** (1968) 629.
7. F. ERDOGAN and T. S. COOK, *Int. J. Fract.* **10** (1974) 629.

8. A. V. VIRKAR and M. R. PLICHTA, *J. Amer. Ceram. Soc.* **66** (1983) 451.
9. W. B. HILLIA and R. J. CHARLES, in "High Strength Materials", edited by V. F. Zackay (Wiley, New York, 1964) pp. 682–701.
10. N. F. MOTT, *Engineering* **165** (1948) 16.
11. J. P. BERRY, *J. Mech. Phys. Solids* **8** (1960) 207.
12. J. P. SINGH, *J. Amer. Ceram. Soc.* **62** (1979) 179.
13. F. ERDOGAN and G.D. GUPTA, *Int. J. Fract.* **11** (1975) 13.
14. F. ERDOGAN and V. BIRICIKOGLU, *Int. J. Engng Sci.* **11** (1973) 745.

Received 7 January
and accepted 25 June 1992